

NUWC-NPT Technical Report 11,781
3 January 2007

Dynamic Response of an Insonified Sonar Window Interacting with a Tonpilz Transducer Array

Andrew J. Hull
Autonomous Systems and Technology Department



**Naval Undersea Warfare Center Division
Newport, Rhode Island**

Approved for public release; distribution is unlimited.


PREFACE

The work described in this report was sponsored by the Office of Naval Research (ONR) under the project "Broadband Acoustic Window Designs for Heavyweight and Lightweight Torpedoes," ONR Project Number 07PR01253-00, program manager David Drumheller (ONR Code 332).

The technical reviewer for this report was Benjamin A. Cray (Code 821).

The author is indebted to Stephen C. Butler (Code 1516) and John B. Blottman (Code 1516) for their discussions on Tonpiz transducer behavior

Reviewed and Approved: 3 January 2007



James S. Griffin
Head, Autonomous Systems and Technology Department



REPORT DOCUMENTATION PAGE

Form Approved
OMB No. 0704-0188

Public reporting for this collection of information is estimated to average 1 hour per response, including the time for reviewing instructions, searching existing data sources, gathering and maintaining the data needed, and completing and reviewing the collection of information. Send comments regarding this burden estimate or any other aspect of this collection of information, including suggestions for reducing this burden, to Washington Headquarters Services, Directorate for Information Operations and Reports, 1215 Jefferson Davis Highway, Suite 1204, Arlington, VA 22202-4302, and to the Office of Management and Budget, Paperwork Reduction Project (0704-0188), Washington, DC 20503.

| | | |
|---|---|---|
| 1. AGENCY USE ONLY (Leave blank) | 2. REPORT DATE 3 January 2007 | 3. REPORT TYPE AND DATES COVERED |
|---|---|---|

| | |
|--|---------------------------|
| 4. TITLE AND SUBTITLE Dynamic Response of an Insonified Sonar Window Interacting with a Tonpilz Transducer Array | 5. FUNDING NUMBERS |
|--|---------------------------|

| | |
|---|--|
| 6. AUTHOR(S) Andrew J. Hull | |
|---|--|

| | |
|---|---|
| 7. PERFORMING ORGANIZATION NAME(S) AND ADDRESS(ES) Naval Undersea Warfare Center Division 1176 Howell Street Newport, RI 02841-1708 | 8. PERFORMING ORGANIZATION REPORT NUMBER TR 11781 |
|---|---|

| | |
|---|---|
| 9. SPONSORING/MONITORING AGENCY NAME(S) AND ADDRESS(ES) Office of Naval Research 875 North Randolph Street Suite 1425 Arlington, VA 22203-1995 | 10. SPONSORING/MONITORING AGENCY REPORT NUMBER |
|---|---|

| |
|--------------------------------|
| 11. SUPPLEMENTARY NOTES |
|--------------------------------|

| | |
|---|-------------------------------|
| 12a. DISTRIBUTION/AVAILABILITY STATEMENT | 12b. DISTRIBUTION CODE |
|---|-------------------------------|

| |
|---|
| 13. ABSTRACT (Maximum 200 words) This report derives and evaluates an analytical model of a sonar window in contact with an array of Tonpilz transducers. The window is fully elastic so that all wave components are present in the analysis. The system is insonified with a plane acoustic wave so that the sonar system is operating in an acoustic receive mode. The output of the model is a transfer function of a transducer element output voltage divided by input pressure versus arrival angle and frequency. This model is intended for analysis of sonar systems that are to be built or modified for broadband processing. The model is validated at low frequency with a comparison to a previously derived thin plate model. Once this is done, an example problem is studied so that the effects of higher order wave interaction with acoustic reception can be understood. It was found that these higher order waves can cause multiple nulls in the acoustic cone and that their locations in the arrival angle-frequency plane can be determined. The effect of these nulls in the beam pattern of the array is demonstrated. This analysis is beneficial because it shows where a sonar system can operate without being adversely effected by dynamic effects in the sonar window. |
|---|

| | |
|--|----------------------------------|
| 14. SUBJECT TERMS Sonar System Tonpilz Transducers Arrays | 15. NUMBER OF PAGES 38 |
| | 16. PRICE CODE |

| | | | |
|--|---|--|--|
| 17. SECURITY CLASSIFICATION OF REPORT Unclassified | 18. SECURITY CLASSIFICATION OF THIS PAGE Unclassified | 19. SECURITY CLASSIFICATION OF ABSTRACT Unclassified | 20. LIMITATION OF ABSTRACT SAR |
|--|---|--|--|

TABLE OF CONTENTS

| Section | Page |
|---|------|
| 1 INTRODUCTION | 1 |
| 2 SYSTEM MODEL..... | 3 |
| 3 TRANSFORMATION INTO THE WAVENUMBER-FREQUENCY DOMAIN | 9 |
| 4 ANALYTICAL SOLUTION..... | 13 |
| 5 MODEL VALIDATION | 17 |
| 6 A NUMERICAL EXAMPLE..... | 21 |
| 7 CONCLUSIONS..... | 31 |
| 8 REFERENCES | 31 |
| APPENDIX — MATRIX AND VECTOR ENTRIES..... | A-1 |

LIST OF ILLUSTRATIONS

| Figure | Page |
|---|------|
| 1 Sonar Window with Tonpilz Transducers | 3 |
| 2 Model of Sonar Window with Tonpilz Transducers..... | 4 |
| 3 Transfer Function of Transducer Voltage Divided by Input Pressure Versus Wavenumber at a Frequency of 100 Hz (____) Elasticity Theory and (×) Thin Plate Theory | 19 |
| 4 Dispersion Curve Versus Arrival Angle and Frequency | 22 |
| 5 Transfer Function of Transducer Voltage Divided by Input Pressure Versus Arrival Angle and Frequency (Units of dB re volts/ μ Pa)..... | 24 |
| 6 Dispersion Curve Plotted Over the Transfer Function | 25 |

LIST OF ILLUSTRATIONS (Cont'd)

| Figure | Page |
|--------|--|
| 7 | Transfer Function of Transducer Voltage Divided by Input Pressure Versus Arrival Angle at (a) 1500 Hz, (b) 2610 Hz, (c) 4030 Hz, and (d) 7320 Hz (____) Magnitude and (- - -) Phase Angle.....26 |
| 8 | Beamformed Response at 1500 Hz with a Steer Angle of 0° (____) Tonpilz Array with Window and (_ _ _ _) Tonpilz Array without Window27 |
| 9 | Beamformed Response at 1500 Hz with a Steer Angle of 30° (____) Tonpilz Array with Window and (_ _ _ _) Tonpilz Array without Window27 |
| 10 | Beamformed Response at 2610 Hz with a Steer Angle of 0° (____) Tonpilz Array with Window and (_ _ _ _) Tonpilz Array without Window28 |
| 11 | Beamformed Response at 2610 Hz with a Steer Angle of 45.1° (____) Tonpilz Array with Window and (_ _ _ _) Tonpilz Array without Window28 |
| 12 | Beamformed Response at 4030 Hz with a Steer Angle of 0° (____) Tonpilz Array with Window and (_ _ _ _) Tonpilz Array without Window29 |
| 13 | Beamformed Response at 4030 Hz with a Steer Angle of 12.5° (____) Tonpilz Array with Window and (_ _ _ _) Tonpilz Array without Window29 |
| 14 | Beamformed Response at 7320 Hz with a Steer Angle of 0° (____) Tonpilz Array with Window and (_ _ _ _) Tonpilz Array without Window30 |
| 15 | Beamformed Response at 7320 Hz with a Steer Angle of 9.8° (____) Tonpilz Array with Window and (_ _ _ _) Tonpilz Array without Window30 |

DYNAMIC RESPONSE OF AN INSONIFIED SONAR WINDOW INTERACTING WITH A TONPILZ TRANSDUCER ARRAY

1. INTRODUCTION

One very typical sonar design consists of a soft material that is in contact with an array of Tonpilz transducers. This soft material is usually called a window (or sometimes a screen). The window serves several purposes: it protects the transducers from water, impact, and debris; it attenuates nonacoustic energy; it provides a safe covering to the sonar system when it is shipped or handled; and it helps to minimize turbulence and hydrodynamic drag. Tonpilz transducers are a reliable transducer design that has been refined for many years. Single resonant Tonpilz transducers typically consist of a head and tail mass separated by piezoelectric stack that emits a voltage when it is subjected to an applied force. Tonpilz transducers are a useful design because they can operate in transmit (active) and receive (passive) mode. They are functional in environments where higher target signal-to-noise ratio is needed than can be obtained from passive sonar only.

Tonpilz transducers have been studied in literature for many years. Basic design guidelines exist in textbooks.¹ General transducer modeling techniques have been previously developed.² Finite element models of the transducers yield the mechanical behavior when it is in contact with a heavy fluid field³ and in contact with air.⁴ Equivalent circuit models have been derived and analyzed.^{5,6,7} Sonar window models have been previously studied. Insertion loss and echo reduction measurements are common in the literature.^{8,9,10} Theoretical analysis has been developed based on thick plate theory.^{9,11,12} Structurally stiffening the window for hull applications has also been investigated.¹³ References 1 through 7 are transducer modeling, and references 8 through 13 are window modeling and testing. It is noted that there is no known analytical model that couples the Tonpilz transducers to a fully elastic sonar window.

This report derives and evaluates an analytical model of a fully elastic sonar window in contact with an array of Tonpilz transducers. The window is insonified by a planewave at varying arrival angles and frequencies. This model is intended for broadband frequency analysis of a sonar system when there is significant interaction between the window and the array of transducers. The formulation of the problem begins with elasticity theory, that models the motion in the window as a combination of dilatational and shear waves. From this theory, expressions for plate displacements in the normal and tangential direction are obtained. The displacements are then inserted into stress relationships and these equations are set equal to the forces acting on the structure by the transducers and the pressure of the incoming acoustic wave. The problem is then written as an algebraic system of equations, in matrix form, where the left-hand terms represent the zero-order window dynamics and are equal to an infinite number of

right-hand terms that represent the forces acting on the structure. Rewriting this zero-order dynamic term, by increasing and decreasing the index, results in an expression for the higher-order modes interacting with the applied forces. The integer shift property is then applied to the right-hand side of all of the terms, resulting in an infinite set of equations that model the wave propagation coefficients of all the modes of the structure. This set of equations is truncated to a finite number of terms, and solutions to the displacement fields are calculated. The transducer output is written as a function of the displacement field at the bottom of the window, and this term is calculated as a transfer function of voltage divided by applied pressure versus arrival angle and frequency. A numerical example is included where the array beam pattern is generated at several frequencies and the results are discussed.

2. SYSTEM MODEL

The system model is that of a sonar window attached to an array of Tonpilz transducers, as shown in figure 1. This mechanical problem is analytically modeled by assuming the sonar window is a fully elastic plate and the Tonpilz transducers are discrete mass-spring-mass systems, as shown in figure 2. The plate (or sonar window) has a thickness of h (m) and is loaded on the top surface with a normal (pressure) forcing function. The transducers on the bottom of the window are equally spaced at a distance of L (m) in the x -direction and each has a head mass per unit length M_H (kg/m), tail mass per unit length M_T (kg/m), and stiffness per unit length K_S (N/m²). The model uses the following assumptions: (1) the forcing function acting on the plate is a planewave at a definite wavenumber and frequency; (2) motion is normal and tangential to the plate in one direction (two-dimensional system); (3) the plate has infinite spatial extent in the x -direction; (4) the head mass has translational degrees of freedom in the x - and z -directions; (5) the tail mass and the spring have translational degrees of freedom in the z -direction; (6) the particle motion is linear; and (7) the fluid medium is lossless.

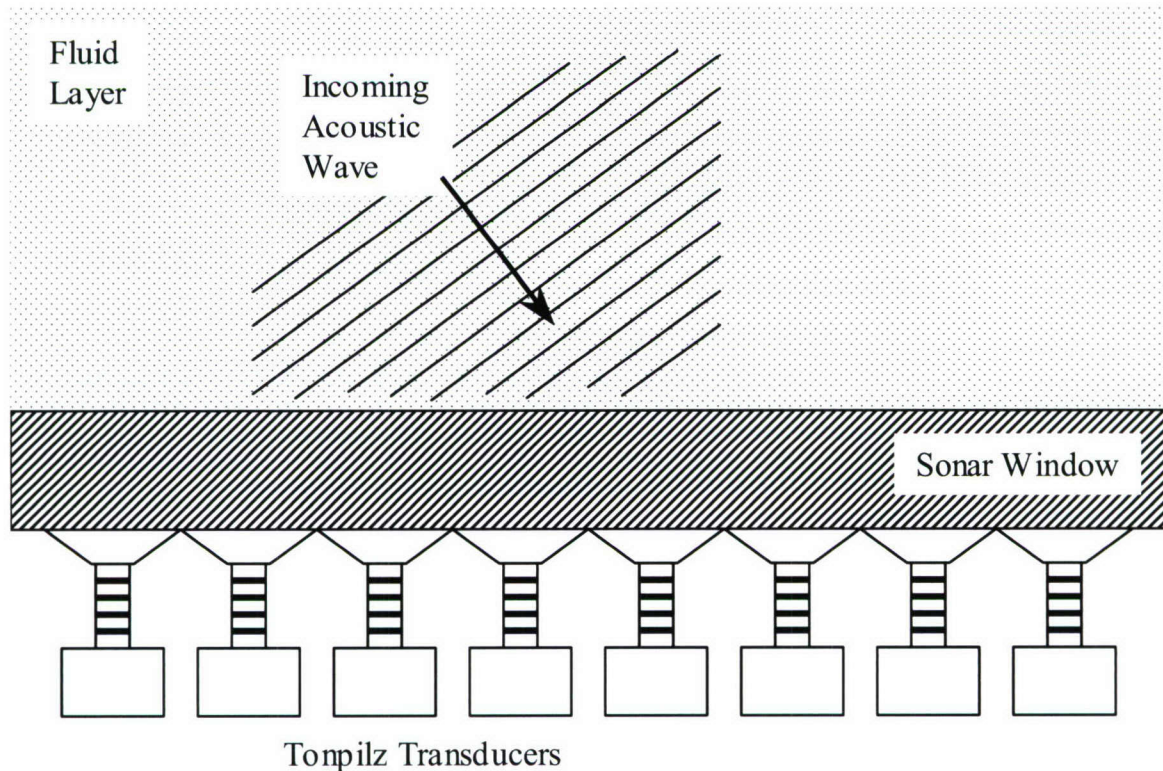


Figure 1. Sonar Window with Tonpilz Transducers

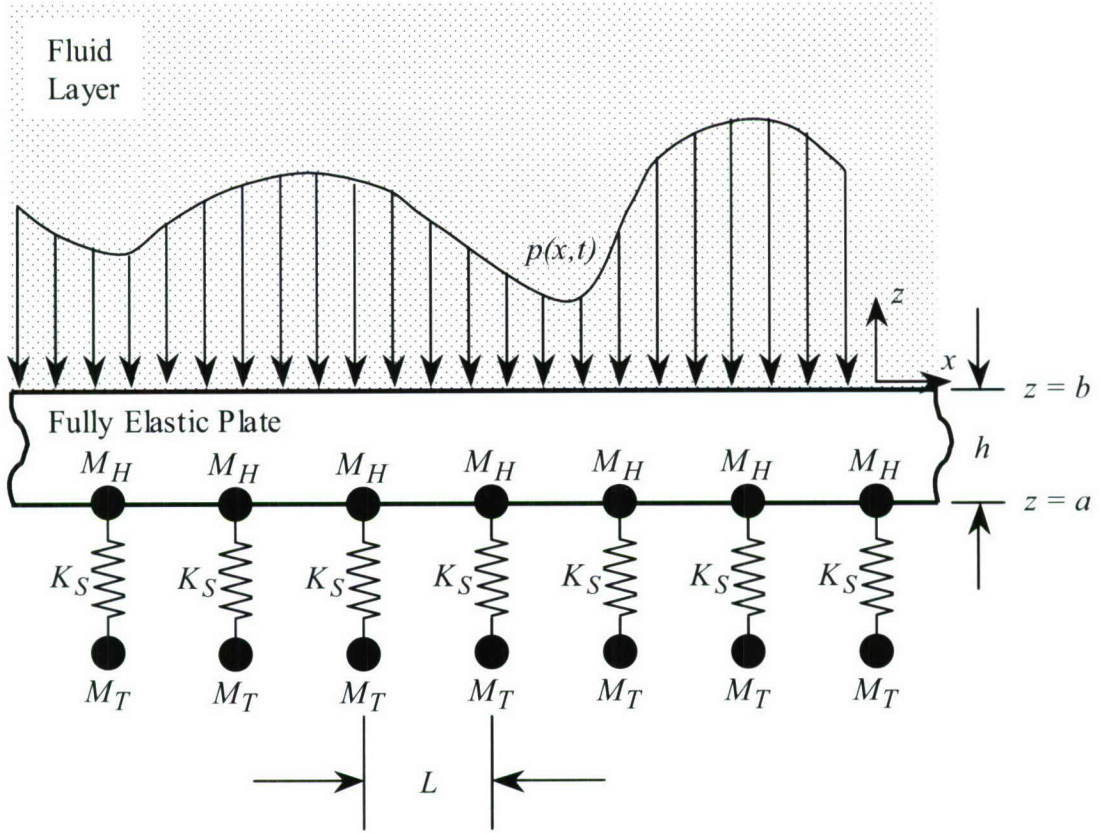


Figure 2. Model of Sonar Window with Tonpilz Transducers

The motion of the elastic plate is governed by the equation

$$\mu \nabla^2 \mathbf{u}(x, y, z, t) + (\lambda + \mu) \nabla \nabla \cdot \mathbf{u}(x, y, z, t) = \rho \frac{\partial^2 \mathbf{u}(x, y, z, t)}{\partial t^2}, \quad (1)$$

where ρ is the density (kg/m^3), λ and μ are the complex Lamé constants (N/m^2), t is time (seconds), \cdot denotes a vector dot product, and $\mathbf{u}(x, y, z, t)$ is the three-dimensional Cartesian coordinate displacement vector and is written as

$$\mathbf{u}(x, y, z, t) = \begin{Bmatrix} u_x(x, y, z, t) \\ u_y(x, y, z, t) \\ u_z(x, y, z, t) \end{Bmatrix} = \nabla \phi(x, y, z, t) + \nabla \times \begin{Bmatrix} \psi_x(x, y, z, t) \\ \psi_y(x, y, z, t) \\ \psi_z(x, y, z, t) \end{Bmatrix}, \quad (2)$$

where ϕ is a dilatational scalar potential, ∇ is the gradient operator, \times denotes a vector crossproduct, and $\vec{\psi}$ is an equivoluminal vector potential. The formulation is now condensed into a two-dimensional problem; thus, $u_y \equiv 0$ and $\partial(\cdot)/\partial y \equiv 0$. Expanding equation (2) and breaking the displacement vector into its individual nonzero terms yields

$$u_x(x, z, t) = \frac{\partial \phi(x, z, t)}{\partial x} - \frac{\partial \psi_y(x, z, t)}{\partial z} \quad (3)$$

and

$$u_z(x, z, t) = \frac{\partial \phi(x, z, t)}{\partial z} + \frac{\partial \psi_y(x, z, t)}{\partial x}. \quad (4)$$

Equations (3) and (4) are next inserted into equation (1), which results in two decoupled wave equations given by

$$c_d^2 \nabla^2 \phi(x, z, t) = \frac{\partial^2 \phi(x, z, t)}{\partial t^2} \quad (5)$$

and

$$c_s^2 \nabla^2 \psi_y(x, z, t) = \frac{\partial^2 \psi_y(x, z, t)}{\partial t^2}, \quad (6)$$

where equation (5) corresponds to the dilatational component and equation (6) corresponds to the shear component of the displacement field. Correspondingly, the constants c_d and c_s are the complex dilatational and shear wavespeeds (m/s), respectively, and are determined by

$$c_d = \sqrt{\frac{\lambda + 2\mu}{\rho}} \quad (7)$$

and

$$c_s = \sqrt{\frac{\mu}{\rho}}. \quad (8)$$

The equations of motion are formulated as a boundary value problem using four equations of stress written in terms of the plates' displacements and corresponding forcing functions. The plate is loaded by a normal (pressure) forcing function as shown in figure 2; thus, the normal stress at $z = b$ is written using a force balance between the pressure in the fluid and the plate as

$$\tau_{zz}(x, b, t) = (\lambda + 2\mu) \frac{\partial u_z(x, b, t)}{\partial z} + \lambda \frac{\partial u_x(x, b, t)}{\partial x} = -p_a(b, x, t), \quad (9)$$

where $p_a(x, t)$ is the pressure field in contact with the top of the plate (N/m^2). The tangential stress on the top of the plate is modeled as a free boundary condition and is written as

$$\tau_{zx}(x, b, t) = \mu \left[\frac{\partial u_x(x, b, t)}{\partial z} + \frac{\partial u_z(x, b, t)}{\partial x} \right] = 0. \quad (10)$$

The plate is loaded by the forces in the Tonpilz transducers' head masses acting on the bottom of the plate, thus, the normal stress at $z = a$ is

$$\tau_{zz}(x, a, t) = (\lambda + 2\mu) \frac{\partial u_z(x, a, t)}{\partial z} + \lambda \frac{\partial u_x(x, a, t)}{\partial x} = \sum_{n=-\infty}^{n=\infty} f_z(a, t) \delta(x - nL), \quad (11)$$

where $f_z(a, t)$ is the force per unit length that each Tonpilz transducer exerts on the plate in the z -direction and $\delta(x - nL)$ is the Dirac delta function that distributes the transducer forces discretely and periodically. Similarly, the tangential stress on the bottom of the plate is

$$\tau_{zx}(x, a, t) = \mu \left[\frac{\partial u_x(x, a, t)}{\partial z} + \frac{\partial u_z(x, a, t)}{\partial x} \right] = \sum_{n=-\infty}^{n=\infty} f_x(a, t) \delta(x - nL), \quad (12)$$

where $f_x(a, t)$ is the force per unit length that each Tonpilz transducer exerts on the plate in the x -direction.

The acoustic pressure in the fluid medium is governed by the two-dimensional wave equation and is written in Cartesian coordinates as

$$\frac{\partial^2 p_a(x, z, t)}{\partial z^2} + \frac{\partial^2 p_a(x, z, t)}{\partial x^2} - \frac{1}{c_f^2} \frac{\partial^2 p_a(x, z, t)}{\partial t^2} = 0, \quad (13)$$

where $p_a(x, z, t)$ is the pressure (N/m²) and c_f is the real valued compressional wavespeed in the fluid (m/s). The interface between the fluid and solid surface at $z = b$ satisfies the linear momentum equation, which relates the acceleration of the plate surface to the spatial gradient of the pressure field by

$$\rho_f \frac{\partial^2 u_z(x, b, t)}{\partial t^2} = - \frac{\partial p_a(x, b, t)}{\partial z}, \quad (14)$$

where ρ_f is the density of the fluid (kg/m³).

The system output is a transfer function of transducer voltage divided by incident pressure, commonly called receive voltage sensitivity (rvs). This is equal to

$$rvs(x, t) = g_{33} t f_s(x, t), \quad (15)$$

where g_{33} is the material constant that relates the mechanical force to electrical output (volts m/N), t is the thickness of each piezoelectric piece from the transducer stack, and $f_s(x, t)$ is the force in the transducer, which, in the case of this model, is the force across the spring.

3. TRANSFORMATION INTO THE WAVENUMBER-FREQUENCY DOMAIN

The problem is now transformed into the wavenumber-frequency domain ($k\omega$) by using the functional form, where the field variables are equal to an unknown function in the z -direction times an exponential function in the x -direction times an exponential function in time. The function in the z -direction is also a function of wavenumber and frequency. The displacements become

$$u_x(x, z, t) = U_x(k, z, \omega) \exp(ikx) \exp(i\omega t) \quad (16)$$

and

$$u_z(x, z, t) = U_z(k, z, \omega) \exp(ikx) \exp(i\omega t), \quad (17)$$

and the pressure is written as

$$p_a(x, z, t) = P_a(z, k, \omega) \exp(ikx) \exp(i\omega t), \quad (18)$$

where $i = \sqrt{-1}$, k is the wavenumber with respect to the x -axis (rad/m) and ω is frequency (rad/s).

Inserting equations (16) and (17) into equations (2) through (6) and solving the differential equations gives the transformed displacement field in the x -direction as

$$U_x(k, z, \omega) = A(k, \omega) i k \exp(i\alpha z) + B(k, \omega) i k \exp(-i\alpha z) + C(k, \omega) i \beta \exp(i\beta z) + D(k, \omega) i \beta \exp(-i\beta z) \quad (19)$$

and the transformed displacement field in the z -direction as

$$U_z(k, z, \omega) = A(k, \omega) i \alpha \exp(i\alpha z) - B(k, \omega) i \alpha \exp(-i\alpha z) + C(k, \omega) i k \exp(i\beta z) + D(k, \omega) i k \exp(-i\beta z), \quad (20)$$

where $A(k, \omega)$, $B(k, \omega)$, $C(k, \omega)$, and $D(k, \omega)$ are unknown complex wave propagation coefficients of the plate, α is the modified wavenumber (rad/m) associated with the dilatational wave and is expressed as

$$\alpha = \sqrt{k_d^2 - k^2} \quad (21)$$

where k_d is the dilatational wavenumber and is equal to ω/c_d ; β is the modified wavenumber (rad/m) associated with the shear wave and is expressed as

$$\beta = \sqrt{k_s^2 - k^2}, \quad (22)$$

where k_s is the shear wavenumber (rad/m) and is equal to ω/c_s .

Inserting equation (18) into (13) and solving the resulting ordinary differential equation yields the transformed pressure field as

$$P_a(z, k, \omega) = M(k, \omega) \exp(i\gamma z) + P_I(\omega) \exp(-i\gamma z), \quad (23)$$

where the first term on the right-hand side represents the outgoing reradiated pressure field caused by the plate displacement and the second term represents the incoming applied incident pressure field (the forcing function) acting on the structure. In equation (23), γ is the modified wavenumber (rad/m) associated with the fluid and is expressed as

$$\gamma = \sqrt{(\omega/c_f)^2 - k^2} = \sqrt{k_f^2 - k^2}, \quad (24)$$

where γ is purely real or imaginary, depending on the sign of the argument under the radical. When the sign of the argument is positive, the analysis is in the acoustic cone; when the sign of the argument is negative, the analysis is in the nonacoustic region. For acoustic sonar response, the analysis is typically studied in the acoustic cone. The relationship between the arrival angle of an acoustic wave and its wavenumber is

$$k = (\omega/c_f) \sin(\theta), \quad (25)$$

where θ is the arrival angle of an incoming acoustic wave (rad) with 0 corresponding to broadside excitation.

The forces exerted by the Tonpilz transducers can be determined with a dynamical model of a mass-spring-mass system. The force per unit length in the z -direction for each transducer is

$$\begin{aligned}
f_z(a,t) &= \left[\frac{\omega^4 M_H M_T - \omega^2 K_S (M_T + M_H)}{K_S - \omega^2 M_T} \right] U_z(k, a, \omega) \exp(ikx) \exp(i\omega t) \\
&= F_z(\omega) U_z(k, a, \omega) \exp(ikx) \exp(i\omega t),
\end{aligned} \tag{26}$$

and the force per unit length in the x -direction for each transducer is

$$\begin{aligned}
f_x(a,t) &= -\omega^2 M_H U_x(k, a, \omega) \exp(ikx) \exp(i\omega t) \\
&= F_x(\omega) U_x(k, a, \omega) \exp(ikx) \exp(i\omega t),
\end{aligned} \tag{27}$$

as the transducer spring constant is zero in the horizontal direction. It is noted that if the transducer is a double or triple resonant type, the expressions given in equations (26) and (27) can be changed to reflect these dynamic effects.

Finally, the output of the transducer can also be transferred into wavenumber-frequency space as

$$r_{vs}(x,t) = RVS(k, \omega) \exp(ikx) \exp(i\omega t). \tag{28}$$

Substituting the spring dynamics yields the receive voltage sensitivity in terms of the displacement at the bottom of the sonar window as

$$RVS(k, \omega) = \left(\frac{\omega^2 M_T}{K_S - \omega^2 M_T} \right) g_{33} t (K_S / w) U_z(k, a, \omega), \tag{29}$$

where w is the width of the transducer head in the x -direction (m).

The four boundary value equations (equations (9) through (12)) are now rewritten in the wavenumber-frequency domain using equations (16) through (27). They become

$$T_{zz}(k, b, \omega) = (\lambda + 2\mu) \frac{\partial U_z(k, b, \omega)}{\partial z} + \lambda \frac{\partial U_x(k, b, \omega)}{\partial x} + \left(\frac{\omega^2 \rho_f}{i\gamma} \right) U_z(k, b, \omega) = -2P_I(\omega), \tag{30}$$

$$T_{zx}(k, b, \omega) = \mu \left[\frac{\partial U_x(k, b, \omega)}{\partial z} + \frac{\partial U_z(k, b, \omega)}{\partial x} \right] = 0, \quad (31)$$

$$T_{zz}(k, a, \omega) = (\lambda + 2\mu) \frac{\partial U_z(k, a, \omega)}{\partial z} + \lambda \frac{\partial U_x(k, a, \omega)}{\partial x} = F_z(\omega) \sum_{n=-\infty}^{n=\infty} U_z(k, a, \omega) \delta(x - nL), \quad (32)$$

and

$$T_{zx}(k, a, \omega) = \mu \left[\frac{\partial U_x(k, a, \omega)}{\partial z} + \frac{\partial U_z(k, a, \omega)}{\partial x} \right] = F_x(\omega) \sum_{n=-\infty}^{n=\infty} U_x(k, a, \omega) \delta(x - nL). \quad (33)$$

4. ANALYTICAL SOLUTION

The analytical solution is now calculated. This begins by transforming the right-hand side of equations (32) and (33) so that the delta functions are absorbed into the displacement functions. This transformation is derived and discussed elsewhere,¹⁴ and produces the following equations

$$F_z(\omega) \sum_{n=-\infty}^{n=\infty} U_z(k, a, \omega) \delta(x - nL) = \frac{F_z(\omega)}{L} \sum_{n=-\infty}^{n=\infty} U_z\left(k + \frac{2\pi n}{L}, a, \omega\right), \quad (34)$$

and similarly

$$F_x(\omega) \sum_{n=-\infty}^{n=\infty} U_x(k, a, \omega) \delta(x - nL) = \frac{F_x(\omega)}{L} \sum_{n=-\infty}^{n=\infty} U_x\left(k + \frac{2\pi n}{L}, a, \omega\right). \quad (35)$$

Next the functional form of the displacements from equations (19) and (20) are inserted into equations (30) through (35) and the following algebraic matrix equation is obtained

$$[\mathbf{A}^{(0)}(k)] \{\mathbf{y}^{(0)}(k)\} = \sum_{n=-\infty}^{n=\infty} [\mathbf{F}^{(n)}(k + \frac{2\pi n}{L})] \{\mathbf{y}^{(n)}(k + \frac{2\pi n}{L})\} + \mathbf{p}, \quad (36)$$

where $[\mathbf{A}^{(0)}(k)]$ is a four by four matrix that models the dynamics of the plate for $n = 0$, $\{\mathbf{y}^{(0)}(k)\}$ is the four by one vector of wave propagation coefficients for $n = 0$, $[\mathbf{F}^{(n)}(k + 2\pi n / L)]$ is the four by four matrix that represents the periodic transducer loading on the structure for n th mode, $\{\mathbf{y}^{(n)}(k + 2\pi n / L)\}$ is the four by one vector of wave propagation coefficients for n th mode, and \mathbf{p} is the four by one vector that models the plane wave excitation. The entries of the matrices and vectors in equation (36) are listed in the appendix. To facilitate a solution to the problem, index shifting is employed. The integer shift property of an infinite summation is applied to equation (36), which, because of the summation from minus infinity to positive infinity, results in

$$\begin{aligned}
& [\mathbf{A}^{(m)}(k + \frac{2\pi m}{L})] \{ \mathbf{y}^{(m)}(k + \frac{2\pi m}{L}) \} \\
&= \sum_{n=-\infty}^{n=\infty} [\mathbf{F}^{(n+m)}(k + \frac{2\pi(n+m)}{L})] \{ \mathbf{y}^{(n+m)}(k + \frac{2\pi(n+m)}{L}) \} + \begin{cases} \mathbf{p} & m = 0 \\ \mathbf{0} & m \neq 0 \end{cases} \\
&= \sum_{m=-\infty}^{m=\infty} [\mathbf{F}^{(m)}(k + \frac{2\pi m}{L})] \{ \mathbf{y}^{(m)}(k + \frac{2\pi m}{L}) \} + \begin{cases} \mathbf{p} & m = 0 \\ \mathbf{0} & m \neq 0. \end{cases}
\end{aligned} \tag{37}$$

where the $\mathbf{0}$ -term is a four by one vector whose entries are zeros. Once the $[\mathbf{A}^{(m)}]$ matrix is integer-indexed and the transducer load matrix indexes have been shifted, the system equations can be rewritten using all the n-indexed modes as

$$\mathbf{A}\mathbf{y} = \mathbf{F}\mathbf{y} + \mathbf{P}, \tag{38}$$

where \mathbf{A} is a block-diagonal matrix and is equal to

$$\mathbf{A} = \begin{bmatrix} \ddots & & \vdots & & \ddots \\ & [\mathbf{A}^{(-1)}(k - \frac{2\pi}{L})] & \mathbf{0} & \mathbf{0} & \\ \dots & \mathbf{0} & [\mathbf{A}^{(0)}(k)] & \mathbf{0} & \dots \\ & \mathbf{0} & \mathbf{0} & [\mathbf{A}^{(1)}(k + \frac{2\pi}{L})] & \\ \ddots & & \vdots & & \ddots \end{bmatrix}, \tag{39}$$

\mathbf{F} is a rank deficient, block-partitioned matrix and is written as

$$\mathbf{F} = \begin{bmatrix} \ddots & & \vdots & & \ddots \\ & [\mathbf{F}^{(-1)}(k - \frac{2\pi}{L})] & [\mathbf{F}^{(0)}(k)] & [\mathbf{F}^{(1)}(k + \frac{2\pi}{L})] & \\ \dots & [\mathbf{F}^{(-1)}(k - \frac{2\pi}{L})] & [\mathbf{F}^{(0)}(k)] & [\mathbf{F}^{(1)}(k + \frac{2\pi}{L})] & \dots \\ & [\mathbf{F}^{(-1)}(k - \frac{2\pi}{L})] & [\mathbf{F}^{(0)}(k)] & [\mathbf{F}^{(1)}(k + \frac{2\pi}{L})] & \\ \ddots & & \vdots & & \ddots \end{bmatrix}, \tag{40}$$

\mathbf{P} is the planewave load vector

$$\mathbf{P} = \left[\dots \quad \mathbf{0}^T \quad \mathbf{p}^T \quad \mathbf{0}^T \quad \dots \right]^T, \quad (41)$$

and \mathbf{y} is the wave propagation coefficient vector that contains all the unknown indexed coefficients as

$$\mathbf{y} = \left[\dots \quad \{\mathbf{y}^{(-1)}(k - \frac{2\pi}{L})\}^T \quad \{\mathbf{y}^{(0)}(k)\}^T \quad \{\mathbf{y}^{(1)}(k + \frac{2\pi}{L})\}^T \quad \dots \right]^T, \quad (42)$$

where the unknown wave propagation coefficients are contained in the equations as

$$\begin{aligned} \{\mathbf{y}^{(0)}(k)\} &= \{A(k, \omega) \quad B(k, \omega) \quad C(k, \omega) \quad D(k, \omega)\}^T \\ &\equiv \{A^{(0)} \quad B^{(0)} \quad C^{(0)} \quad D^{(0)}\}^T. \end{aligned} \quad (43)$$

The $\mathbf{0}$ -term in equation (39) is a four by four matrix whose entries are all zeros and the $\mathbf{0}$ -term in equation (41) is a four by one vector whose entries are all zeros. Equation (38) is assembled, and the wave-propagation coefficients that reside in the \mathbf{y} vector are found by

$$\mathbf{y} = [\mathbf{A} - \mathbf{F}]^{-1} \mathbf{P}. \quad (44)$$

When the coefficients are determined, the displacements of the system can be calculated using equations (19) and (20) and the $n = 0$ wave propagation coefficients.

5. MODEL VALIDATION

The sonar window — Tonpilz transducer interaction model — can be compared and validated for a thin plate at low frequencies using a Bernoulli-Euler model that has been previously developed.^{14,15,16} The stiffeners in these models are replaced by Tonpilz transducer dynamics so that the validation example corresponds to the thick plate model developed in sections 2 through 4. The thin plate model has one degree of freedom that is the displacement in the z -direction. This equation is written as

$$\frac{U_z(k, \omega)}{P_I(\omega)} = 2T(k, \omega) \left[\frac{1 + \frac{F_z(\omega)}{L} T(k, \omega) - \frac{F_z(\omega)}{L} \sum_{n=-\infty}^{n=\infty} T(k + \frac{2\pi n}{L}, \omega)}{1 - \frac{F_z(\omega)}{L} \sum_{n=-\infty}^{n=\infty} T(k + \frac{2\pi n}{L}, \omega)} \right], \quad (45)$$

where

$$T(k, \omega) = \frac{-1}{Dk^4 - \rho h \omega^2 + \left(\frac{\rho_f \omega^2}{i\gamma} \right)}, \quad (46)$$

and

$$D = \frac{Eh^3}{12(1-\nu^2)}, \quad (47)$$

where E is Young's modulus (N/m^2) and ν is Poisson's ratio (dimensionless). Once the normal displacement is known, the transducer output is determined using equation (29).

Figure 3 is a plot of the transfer function of transducer voltage divided by input pressure versus wavenumber at a frequency of 100 Hz. This extremely low frequency was chosen because it is a value at which the two models should theoretically agree. Additionally, the comparison is made versus wavenumber rather than arrival angle so that the higher wavenumber dynamics are included in the comparison. This example was generated with the following system parameters: window thickness h is 0.005 m, window density ρ is 1200 kg/m^3 , Lamé constant λ is $9.31 \times 10^8 \text{ N/m}^2$, Lamé constant μ is $1.03 \times 10^8 \text{ N/m}^2$, fluid density ρ_f is 1000 kg/m^3 ,

fluid compressional wavespeed c_f is 1500 m/s, transducer head mass M_H is 2.5 kg/m, transducer tail mass M_T is 10.0 kg/m, transducer stiffness K_S is 1×10^6 N/m², transducer separation distance L is 0.1 m, transducer face width w is 0.095 m, transducer stack height t is 0.01 m, and transducer constant g_{33} is 0.025 (volts m)/N. In figure 3, the solid line is the elastic plate theory developed in sections 2 through 4 and corresponds to equations (16) through (44); and the \times symbols are the Bernoulli-Euler plate theory and correspond to equations (45) through (47). The elastic plate model was calculated using eleven modes ($-5 < n < 5$) that produced a 20-by 20-element system matrix while the thin plate model was calculated using 51 modes ($-25 < n < 25$). Note that there is agreement between the two models over the entire wavenumber region.

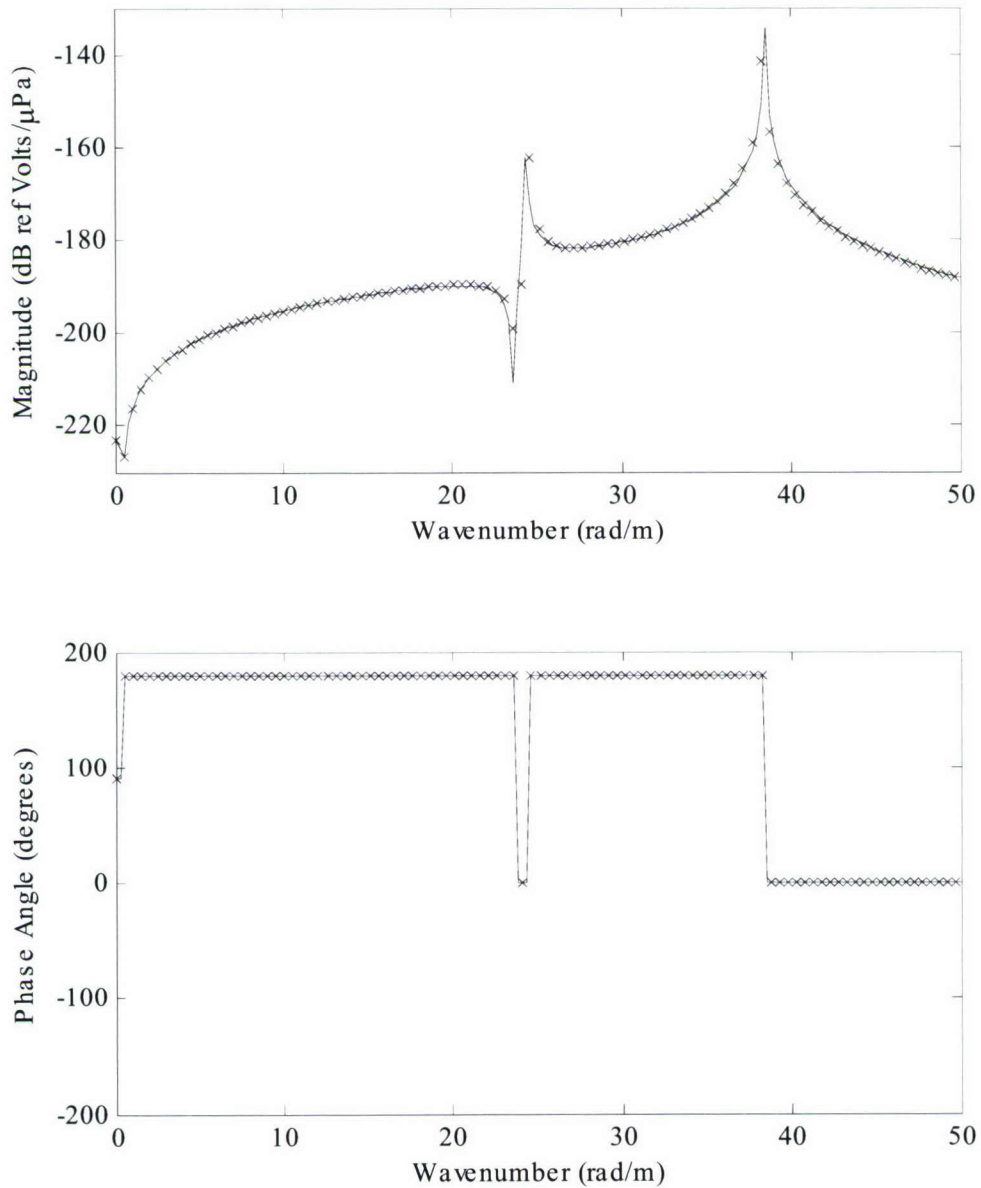


Figure 3. Transfer Function of Transducer Voltage Divided by Input Pressure Versus Wavenumber at a Frequency of 100 Hz
 (—) Elasticity Theory and (x) Thin Plate Theory

6. A NUMERICAL EXAMPLE

A numerical example to illustrate the dynamics of a sonar window interacting with the Tonpiliz transducer array is now presented. To understand fully the model results, it is necessary at this point to slightly digress. The features present in the Tonpiliz transducer output are best understood if the dispersion curve for the system is studied. The dispersion curve is found by setting

$$\det [\mathbf{A} - \mathbf{F}] = 0, \quad (48)$$

and this determines the location in the wavenumber-frequency plane where free wave propagation can exist. Each of these free waves is related to a specific dynamic motion of the system. Figure 4 is the dispersion curve for an example with the following system parameters: window thickness h is 0.1 m, window density ρ is 1200 kg/m³, Lamé constant λ is 1.43×10^9 N/m², Lamé constant μ is 3.57×10^8 N/m², fluid density ρ_f is 1000 kg/m³, fluid compressional wavespeed c_f is 1500 m/s, transducer head mass M_H is 1 kg/m, transducer tail mass M_T is 4 kg/m, transducer stiffness K_S is 1×10^7 N/m², transducer separation distance L is 0.1 m, transducer face width w is 0.095 m, transducer stack height t is 0.01 m, and transducer constant g_{33} is 0.025 (volts m)/N. The noticeable feature from figure 4 is that the system is very rich with free wave propagation above 2490 Hz. This frequency value corresponds to the first antisymmetric Lamb wave of the system. Without the mass-loading, this would occur at

$$f = \frac{c_s}{2h} = 2730 \text{ Hz}; \quad (49)$$

however, because the transducers mass-load the plate, this location is shifted downward in frequency. It is noted that the multiple free waves correspond to higher order plate waves, fluid/structure interaction waves, and the first set of periodic waves, i.e., $n = \pm 1$. These periodic waves are related to the spacing of the individual transducers and occur in wavenumber at integer multiples of

$$k = \frac{2\pi}{L}. \quad (50)$$

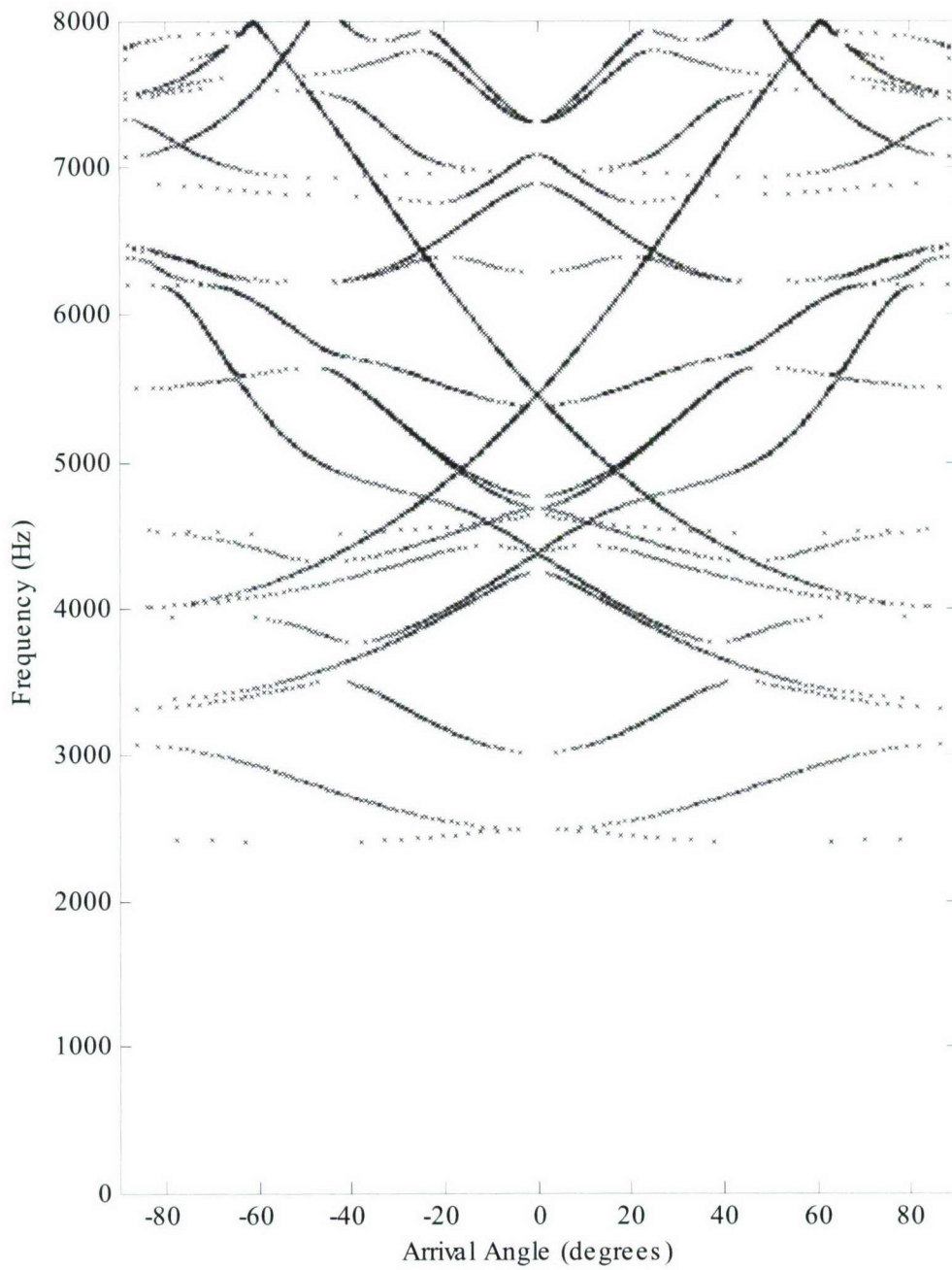


Figure 4. Dispersion Curve Versus Arrival Angle and Frequency

These periodic waves are frequently called Floquet¹⁷ and/or Bloch^{17,18} waves. An additional note to the dispersion curve is included. Although equation (48) may predict a specific free wave, it may not necessarily propagate in the structure. (An acoustic load may not excite a specific free wave, or the excitation may result in an extremely small response.) The propagation of a wave is dependent on the interaction of the structural load with the physics of the free wave.

Figure 5 is a color image of the transfer function of transducer voltage divided by input pressure versus arrival angle and frequency for the example problem. The scale is shown next to the image as a colorbar and corresponds to dB referenced to volts/ μ Pa. The response of the system shown in figure 5 is extremely complex, however, most of the features that are present are nulls. To understand the relationship of these nulls with respect to the free wave propagation, the dispersion curve is plotted over the transfer function in figure 6. The color map scale in figure 6 is the same as that of figure 5. Nulls frequently exist between branches of the dispersion curve that have split or separated. This separation is due to the fluid loading on the plate. Figure 7 is four cuts of figure 5 at 1500, 2610, 4030, and 7320 Hz, respectively, and is shown to illustrate the magnitude (solid line) and phase angle (dashed line) differential versus arrival angle at various frequencies. The last three frequencies are shown to illustrate the nulling effects (or system zero dynamics) that are present at higher frequencies.

Finally, the system response can be beamformed using

$$B(k, \omega) = \sum_{n=1}^N RVS(k, \omega) \exp[i(k - k_s)x_n], \quad (51)$$

where N is the number of sensors in the array, k_s is the steered wavenumber (rad/m), and x_n is the location of the n th sensor (m). For the following analysis, a 16-sensor (element) array is used. The beam patterns are displayed as polar plots, with the solid lines in the plots corresponding to array response based on the theory developed previously (equations (1) through (44)), and the dashed lines are the response of the array to unity input at all wavenumbers. Each short dashed concentric half circle represents 10 dB of energy. Because these beam patterns are being displayed as polar plots, the wavenumbers in equation (51) have been converted into arrival angles. Figure 8 is a plot of the beamformed response at 1500 Hz with a steer angle of 0° . Figure 9 is a plot of the beamformed response at 1500 Hz with a steer angle of 30° . It is noted that in these cases, the sonar window improves the response of the beamformer. This is primarily due to the receive energy drop off at large arrival angles. Figure 10 is a plot of the beamformed response at 2610 Hz with a steer angle of 0° . Again, the sonar window dynamics have improved the beam pattern. Figure 11 is the beamformed response at 2610 Hz with a steer angle of 45.1° , an angle that corresponds to a null in the system response. Steering the array response into this null location has significantly degraded the response of the beamformer. Figure 12 is a plot of the

beamformed response at 4030 Hz with a steer angle of 0° . In this case, the sonar window slightly degrades the beamformer response. Figure 13 is a plot of the beamformed response at 4030 Hz with a steer angle of 12.5° . Steering into the null does not seriously degrade the beamformer response. Figure 14 is a plot of the beamformed response at 7320 Hz with a steer angle of 0° . The sonar window significantly improves the sidelobe response of the array at this frequency and steer angle. Figure 15 is a plot of the beamformed response at 7320 Hz with a steer angle of 9.8° . In this case, the beam pattern has been mildly degraded.

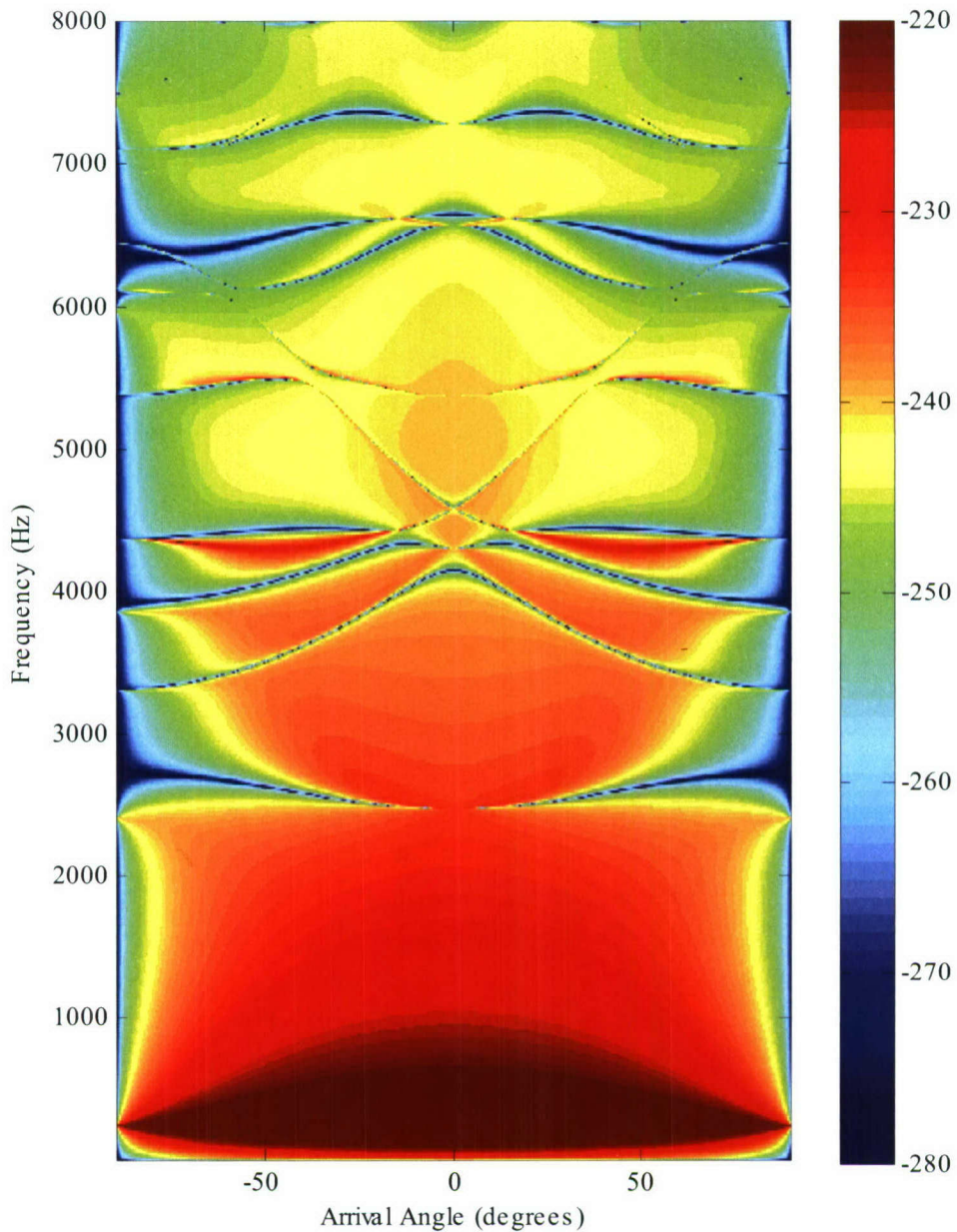


Figure 5. Transfer Function of Transducer Voltage Divided by Input Pressure Versus Arrival Angle and Frequency (Units of dB re volts/ μ Pa)

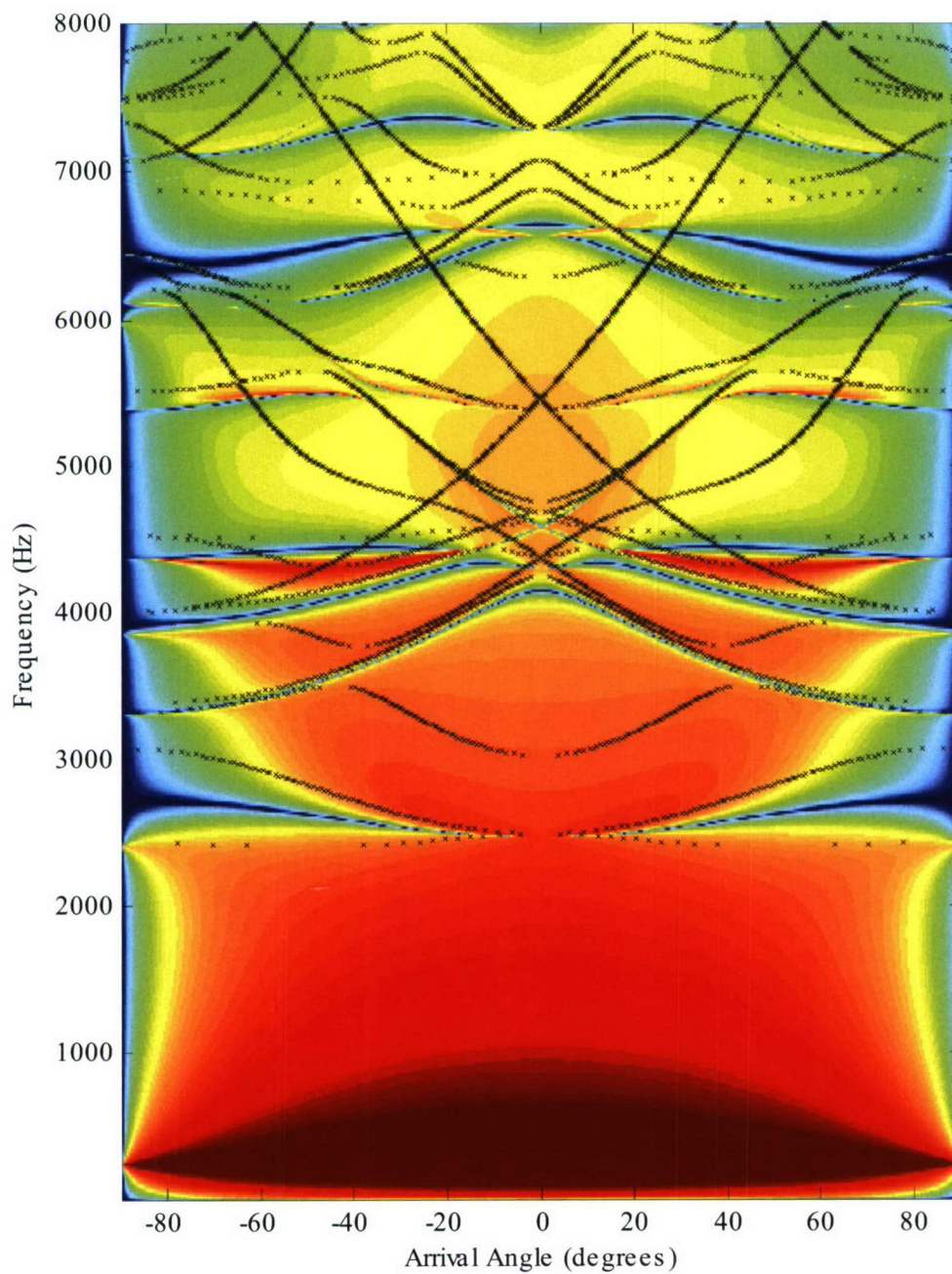


Figure 6. Dispersion Curve Plotted Over the Transfer Function

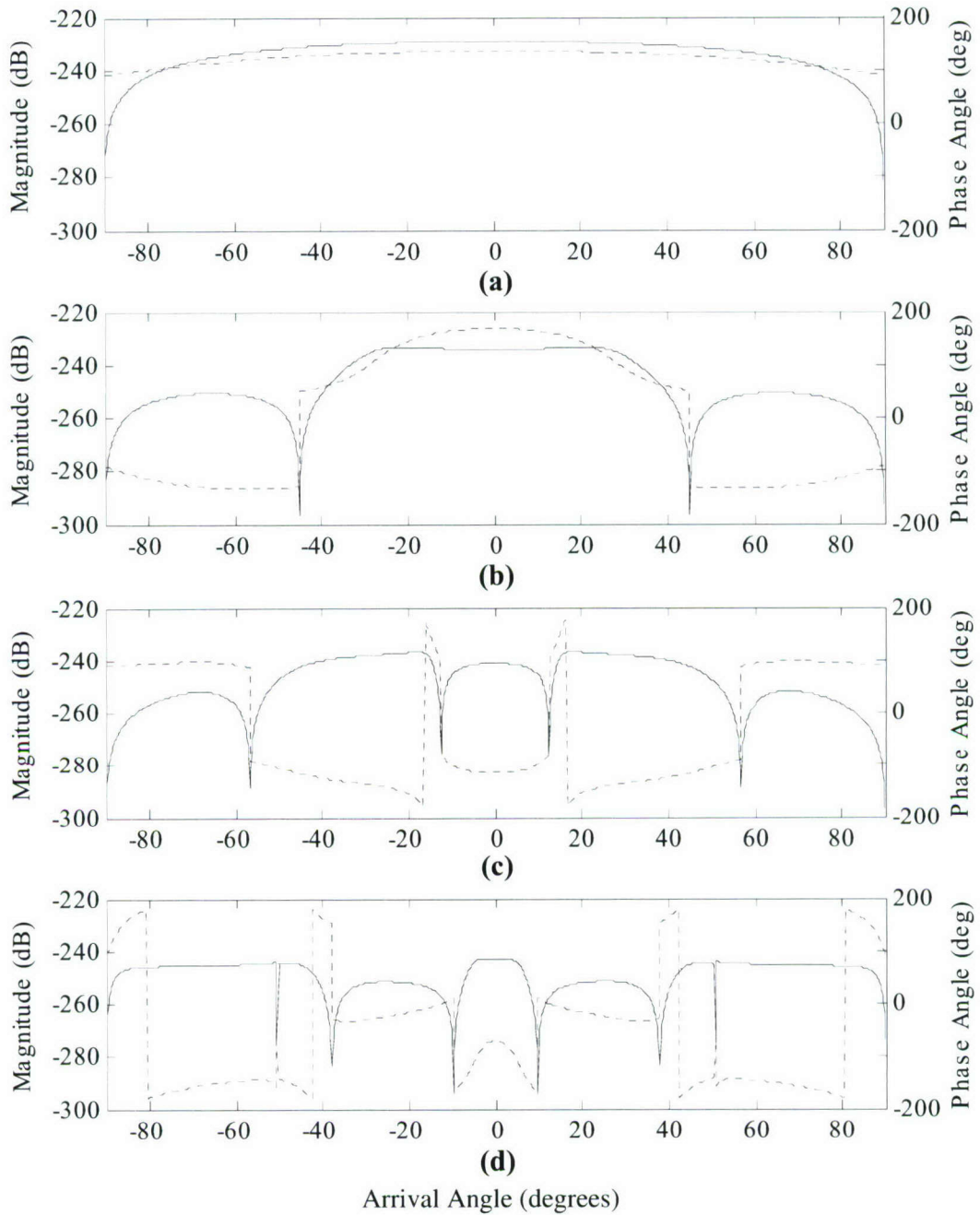


Figure 7. Transfer Function of Transducer Voltage Divided by Input Pressure Versus Arrival Angle at (a) 1500 Hz, (b) 2610 Hz, (c) 4030 Hz, and (d) 7320 Hz (—) Magnitude and (----) Phase Angle

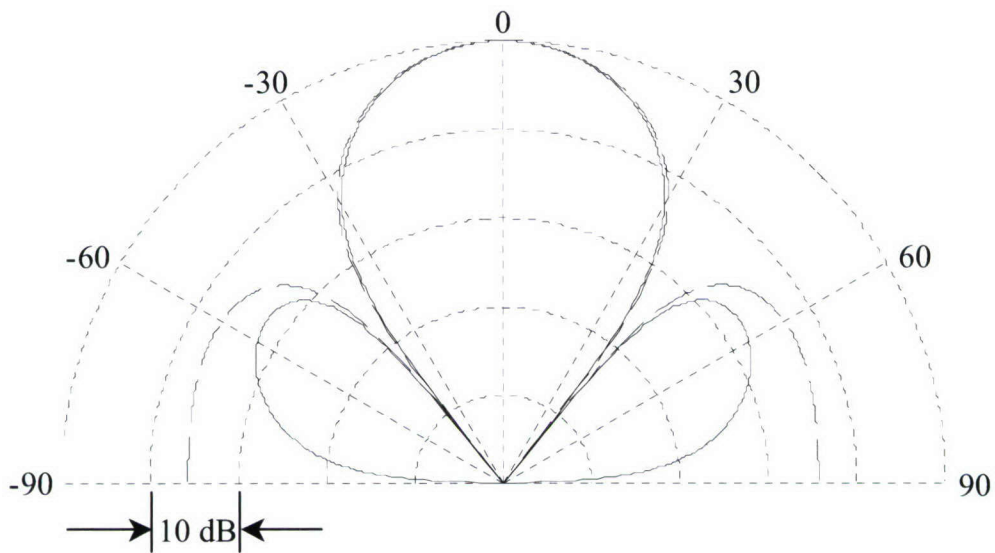


Figure 8. Beamformed Response at 1500 Hz with a Steer Angle of 0°
 (_____) Tonpilz Array with Window and (- - - -) Tonpilz Array without Window

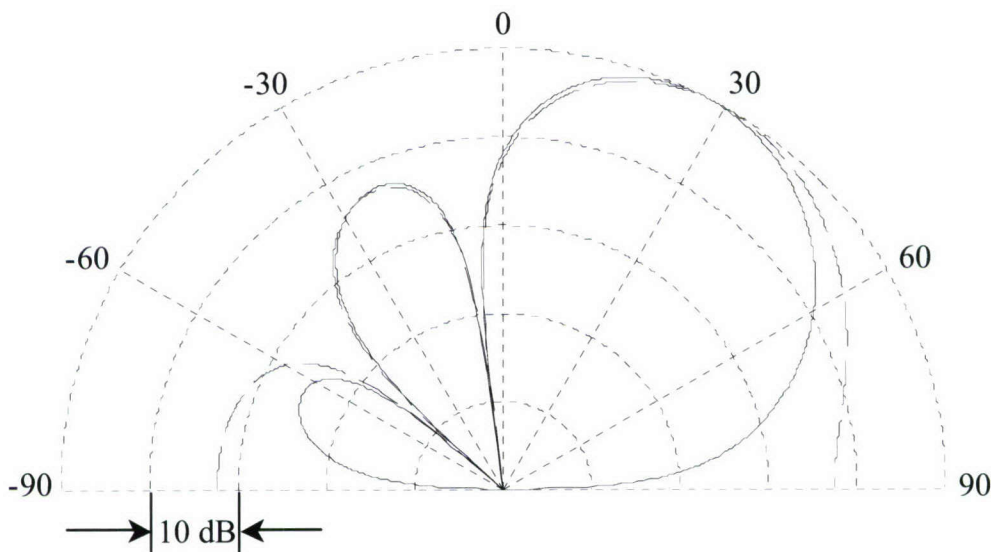


Figure 9. Beamformed Response at 1500 Hz with a Steer Angle of 30°
 (_____) Tonpilz Array with Window and (- - - -) Tonpilz Array without Window

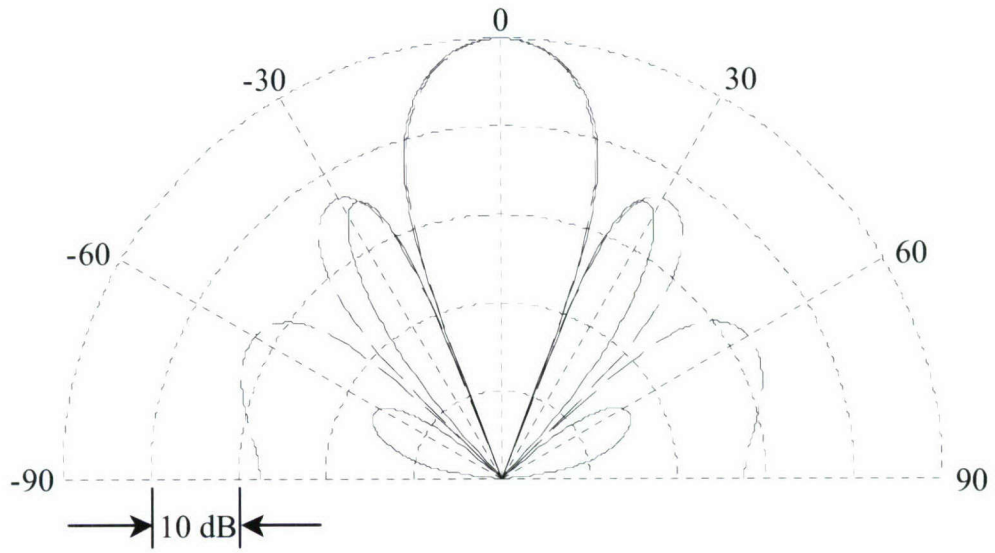


Figure 10. Beamformed Response at 2610 Hz with a Steer Angle of 0°
 (_____) Tonpilz Array with Window and (- - - -) Tonpilz Array without Window

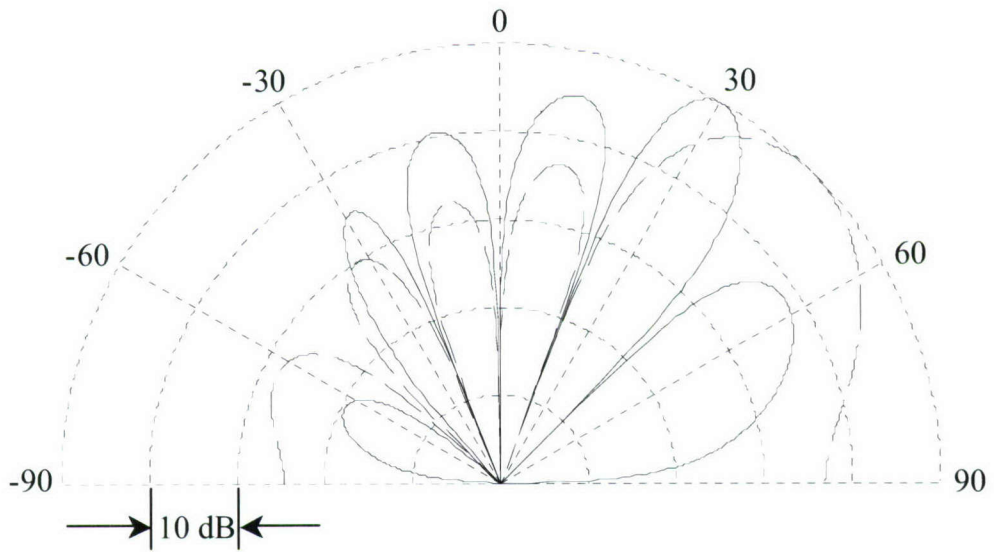


Figure 11. Beamformed Response at 2610 Hz with a Steer Angle of 45.1°
 (_____) Tonpilz Array with Window and (- - - -) Tonpilz Array without Window

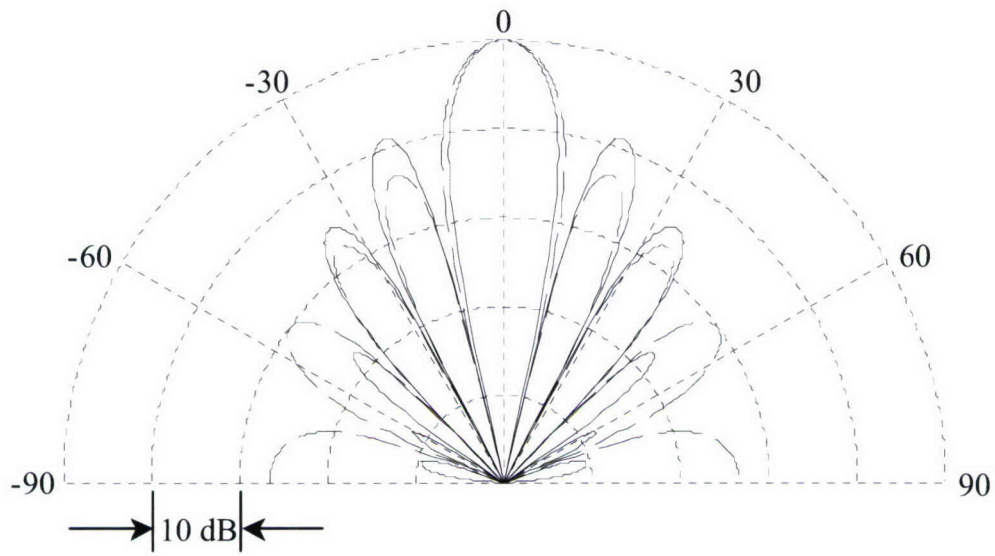


Figure 12. Beamformed Response at 4030 Hz with a Steer Angle of 0°
 (—) Tonpilz Array with Window and (- - -) Tonpilz Array without Window

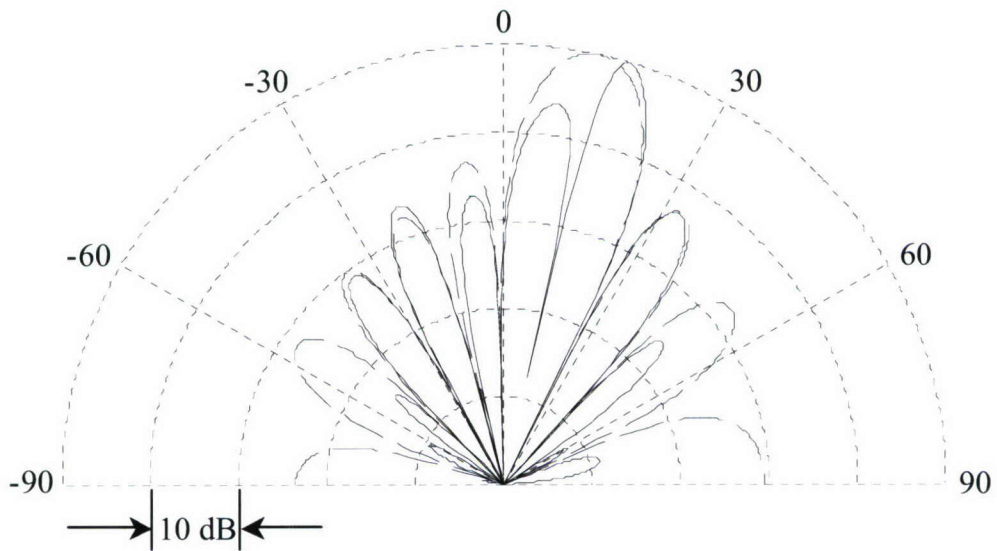


Figure 13. Beamformed Response at 4030 Hz with a Steer Angle of 12.5°
 (—) Tonpilz Array with Window and (- - -) Tonpilz Array without Window

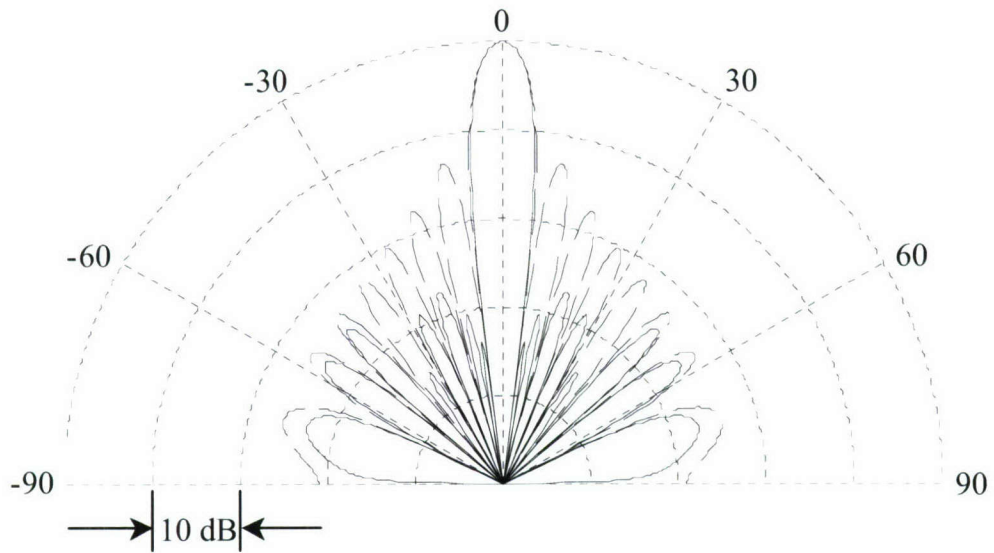


Figure 14. Beamformed Response at 7320 Hz with a Steer Angle of 0°
 (—) Tonpilz Array with Window and (- - -) Tonpilz Array without Window

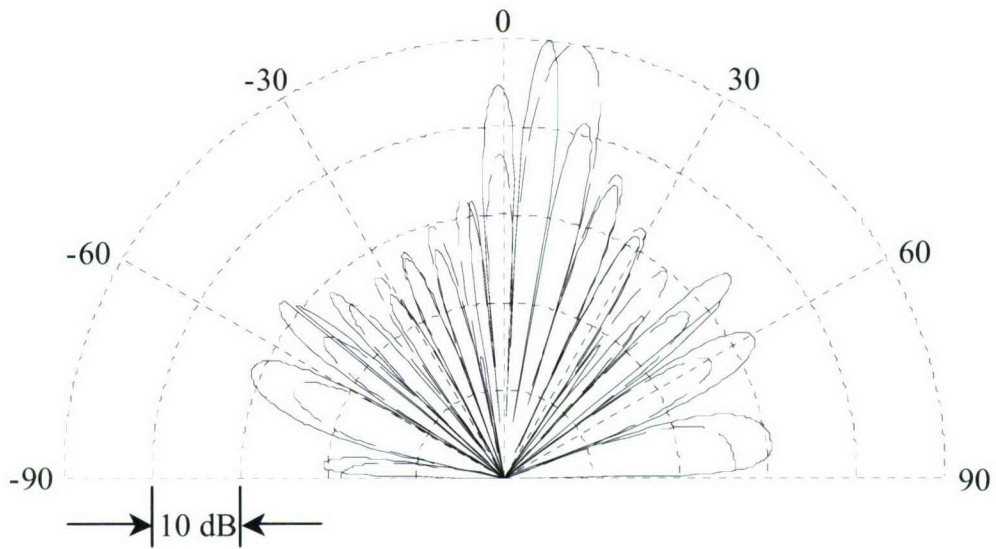


Figure 15. Beamformed Response at 7320 Hz with a Steer Angle of 9.8°
 (—) Tonpilz Array with Window and (- - -) Tonpilz Array without Window

7. CONCLUSIONS

The dynamics of a fully elastic sonar window interacting with an array of single resonant Tonpilz transducers have been analytically modeled. This model shows the effects of acoustic energy insonifying the array at all frequencies, rather than at a single frequency. This is useful as sonar systems are built or modified for broadband processing. The model predicts where the acoustic cone is smooth for optimum sonar processing and where the effects of null responses will enter into the processing. The effect of the sonar window on the beam pattern has been demonstrated.

8. REFERENCES

1. D. Stansfield, *Underwater Electroacoustic Transducers, A Handbook for User and Designers*, Bath University Press and Institute of Acoustics, Bath, United Kingdom, 1991, pp. 179-195.
2. M. P. Johnson, "Equivalent Modal Impedance Matrix of Multiple Degree of Freedom Electroelastic Structures," *Journal of the Acoustical Society of America*, vol. 88, no. 1, 1990, pp. 1-6.
3. Y. Roh and X. Lu, "Design of an Underwater Tonpilz Transducer with 2-2 Mode Piezocomposite Materials," *Journal of the Acoustical Society of America*, vol. 119, no. 6, 2006, pp. 3734-3740.
4. C. Desilets, G. Wojcik, L. Nikodym, and K. Mesterton, "Analysis and Measurements of Acoustically Matched, Air-Coupled Tonpilz Transducers," *Proceedings of IEEE Ultrasonics Symposium*, pp. 1045-1048, 1999.
5. M. B. Moffett, J. M. Powers, and M. D. Jevnager, "A Tonpilz Projector for Use in an Underwater Horn," *Journal of the Acoustical Society of America*, vol. 103, no. 6, 1998, pp. 3353-3361.
6. J. C. Piquette, "Applications of the Method for Transducer Transient Suppression to Various Transducer Types," *Journal of the Acoustical Society of America*, vol. 94(1), no. 2, 1993, pp. 646-651.
7. M. Van Crombrugge and W. Thompson Jr., "Optimization of the Transmitting Characteristics of a Tonpilz-Type Transducer by Proper Choice of Impedance Matching Layers," *Journal of the Acoustical Society of America*, vol. 77, no. 2, 1985, pp. 747-752.

8. C. M. Thompson, "Development of a Structurally Rigid, Acoustically Transparent Plastic," *Journal of the Acoustical Society of America*, vol. 87, no. 3, 1990, pp. 1138-1143.
9. D. L. Folds and C. D. Loggins, "Transmission and Reflection of Ultrasonic Waves in Layered Media," *Journal of the Acoustical Society of America*, vol. 62, no. 5, 1977, pp. 1102-1109.
10. E. E. Mikeska and J. A. Behrens, "Evaluation of Transducer Window Materials," *Journal of the Acoustical Society of America*, vol. 59, no. 6, 1976, pp. 1294-1298.
11. M. Kim and Y. F. Hwang, "An Analysis of Wave Dispersion in Coarsely Laminated Symmetric Composite Plates," *Journal of the Acoustical Society of America*, vol. 100(1), no. 4, 1996, pp. 1981-1991.
12. J. S. Hickman, D. E. Risty, and E. S. Stewart, "Properties of Sandwich-Type Structures as Acoustic Windows," *Journal of the Acoustical Society of America*, vol. 29, no. 7, 1957, pp. 858-864.
13. J. O. R. Blake, R. A. Shenoi, J. House, and T. Turton, "Strength Modeling in Stiffened FRP Structures with Viscoelastic Inserts for Ocean Structures," *Ocean Engineering*, vol. 29, no. 8, 2002, pp. 849-869.
14. B. A. Cray, "Acoustic Radiation from Periodic and Sectionally Aperiodic Rib-Stiffened Plates," *Journal of the Acoustical Society of America*, vol. 95, no. 1, 1994, pp. 256-264.
15. B. R. Mace, "Periodically Stiffened Fluid-Loaded Plates, I: Response to Convected Harmonic Pressure and Free Wave Propagation," *Journal of Sound and Vibration*, vol. 73, no. 4, 1980, pp. 473-486.
16. B. R. Mace, "Periodically Stiffened Fluid-Loaded Plates, II: Response to Line and Point Forces," *Journal of Sound and Vibration*, vol. 73 no. 4, 1980, pp. 487-504.
17. M. Tran-Van-Nhieu, "Scattering from a Ribbed Finite Cylindrical Shell with Internal Axisymmetric Oscillators," *Journal of the Acoustical Society of America*, vol. 112, no. 2, 2002, pp. 402-410.
18. D. M. Photiadis, "The Effect of Irregularity on the Scattering of Acoustic Waves from a Ribbed Plate," *Journal of the Acoustical Society of America*, vol. 91(1), no. 4, 1992, pp. 1897-1903.

**APPENDIX
MATRIX AND VECTOR ENTRIES**

The entries of the matrixes and vectors in equation (44) are listed below. Without loss of generality, the top of the plate is defined as $z = b = 0$. For the $[\mathbf{A}^{(n)}(k + 2\pi n / L)]$ matrix, the nonzero entries are

$$a_{11} = -\alpha_n^2 \lambda - 2\alpha_n^2 \mu - \lambda k_n^2 + \frac{\alpha_n \omega^2 \rho_f}{\gamma_n}, \quad (\text{A-1})$$

$$a_{12} = -\alpha_n^2 \lambda - 2\alpha_n^2 \mu - \lambda k_n^2 - \frac{\alpha_n \omega^2 \rho_f}{\gamma_n}, \quad (\text{A-2})$$

$$a_{13} = -2\mu k_n \beta_n + \frac{k_n \omega^2 \rho_f}{\gamma_n}, \quad (\text{A-3})$$

$$a_{14} = 2\mu k_n \beta_n + \frac{k_n \omega^2 \rho_f}{\gamma_n}, \quad (\text{A-4})$$

$$a_{21} = -2\mu k_n \alpha_n, \quad (\text{A-5})$$

$$a_{22} = 2\mu k_n \alpha_n, \quad (\text{A-6})$$

$$a_{23} = \mu(\beta_n^2 - k_n^2), \quad (\text{A-7})$$

$$a_{24} = \mu(\beta_n^2 - k_n^2), \quad (\text{A-8})$$

$$a_{31} = (-\alpha_n^2 \lambda - 2\alpha_n^2 \mu - \lambda k_n^2) \exp(i\alpha_n a), \quad (\text{A-9})$$

$$a_{32} = (-\alpha_n^2 \lambda - 2\alpha_n^2 \mu - \lambda k_n^2) \exp(-i\alpha_n a), \quad (\text{A-10})$$

$$a_{33} = -2\mu k_n \beta_n \exp(i\beta_n a) , \quad (\text{A-11})$$

$$a_{34} = 2\mu k_n \beta_n \exp(-i\beta_n a) , \quad (\text{A-12})$$

$$a_{41} = -2\mu k_n \alpha_n \exp(i\alpha_n a) , \quad (\text{A-13})$$

$$a_{42} = 2\mu k_n \alpha_n \exp(-i\alpha_n a) , \quad (\text{A-14})$$

$$a_{43} = \mu(\beta_n^2 - k_n^2) \exp(i\beta_n a) , \quad (\text{A-15})$$

and

$$a_{44} = \mu(\beta_n^2 - k_n^2) \exp(-i\beta_n a) , \quad (\text{A-16})$$

where

$$k_n = k + \frac{2\pi n}{L} , \quad (\text{A-17})$$

$$\alpha_n = \sqrt{k_d^2 - k_n^2} , \quad (\text{A-18})$$

$$\beta_n = \sqrt{k_s^2 - k_n^2} , \quad (\text{A-19})$$

and

$$\gamma_n = \sqrt{(\omega/c_f)^2 - k_n^2} = \sqrt{k_f^2 - k_n^2} . \quad (\text{A-20})$$

For the $[\mathbf{F}^{(n)}(k + 2\pi n/L)]$ matrix, the nonzero entries are

$$f_{31} = \frac{F_z(\omega)}{L} (i\alpha_n) \exp(i\alpha_n a) , \quad (\text{A-21})$$

$$f_{32} = \frac{F_z(\omega)}{L} (-i\alpha_n) \exp(-i\alpha_n a) , \quad (\text{A-22})$$

$$f_{33} = \frac{F_z(\omega)}{L} (ik_n) \exp(i\beta_n a) , \quad (\text{A-23})$$

$$f_{34} = \frac{F_z(\omega)}{L} (ik_n) \exp(-i\beta_n a) , \quad (\text{A-24})$$

$$f_{41} = \frac{F_x(\omega)}{L} (ik_n) \exp(i\alpha_n a) , \quad (\text{A-25})$$

$$f_{42} = \frac{F_x(\omega)}{L} (ik_n) \exp(-i\alpha_n a) , \quad (\text{A-26})$$

$$f_{43} = \frac{F_x(\omega)}{L} (-i\beta_n) \exp(i\beta_n a) , \quad (\text{A-27})$$

and

$$f_{44} = \frac{F_x(\omega)}{L} (i\beta_n) \exp(-i\beta_n a) . \quad (\text{A-28})$$

The \mathbf{y} vector entries are

$$\mathbf{y} = \{ \dots \quad A^{(-1)} \quad B^{(-1)} \quad C^{(-1)} \quad D^{(-1)} \quad A^{(0)} \quad B^{(0)} \quad C^{(0)} \quad D^{(0)} \quad A^{(1)} \quad B^{(1)} \quad C^{(1)} \quad D^{(1)} \quad \dots \}^T . \quad (\text{A-29})$$

The \mathbf{p} vector entries are

$$\mathbf{p} = \{ -2P_I(\omega) \quad 0 \quad 0 \quad 0 \}^T . \quad (\text{A-30})$$

INITIAL DISTRIBUTION LIST

| Addressee | No. of Copies |
|---|----------------------|
| Office of Naval Research (Code 332 – D. Drumheller) | 2 |
| Defense Technical Information Center | 2 |
| Center for Naval Analyses | 1 |